

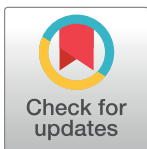
RESEARCH ARTICLE

Fluctuation in residual strain and dissipated energy of saturated sandstone under tiered cyclic loading

Changbao Jiang¹, Guojian Cheng^{1,2}, Minke Duan^{1,3*}, Yufei Chen¹, Yang Yang¹, Qinrong Kang⁴

1 State Key Laboratory of Coal Mine Disaster Dynamics and Control, Chongqing University, Chongqing, China, **2** China Coal Technology Engineering Group Chongqing Research Institute, Chongqing, China, **3** Department of Geology and Petroleum Geology, School of Geosciences, University of Aberdeen, Aberdeen AB24 3UE, United Kingdom, **4** School of Xingfa Mining and Civil Engineering, Wuhan Institute of Technology, Wuhan, Hubei, China

* minkeduan@cqu.edu.cn



OPEN ACCESS

Citation: Jiang C, Cheng G, Duan M, Chen Y, Yang Y, Kang Q (2020) Fluctuation in residual strain and dissipated energy of saturated sandstone under tiered cyclic loading. PLoS ONE 15(7): e0236335. <https://doi.org/10.1371/journal.pone.0236335>

Editor: Jianguo Wang, China University of Mining and Technology, CHINA

Received: January 10, 2020

Accepted: July 3, 2020

Published: July 24, 2020

Copyright: © 2020 Jiang et al. This is an open access article distributed under the terms of the [Creative Commons Attribution License](https://creativecommons.org/licenses/by/4.0/), which permits unrestricted use, distribution, and reproduction in any medium, provided the original author and source are credited.

Data Availability Statement: All relevant data are within the manuscript and its Supporting Information files.

Funding: This study was financially supported by the National Natural Science Foundation of China (51674048). The first author also acknowledges the financial support provided by the China Scholarship Council (CSC).

Competing interests: The authors have declared that no competing interests exist.

Abstract

To study the influence of cyclic stress on the nonlinear behavior of saturated sandstone, the residual strain properties and energy dissipation characteristics of the sandstone under tiered cyclic loading were experimentally investigated. The axial/radial residual deformation and energy dissipation characteristics of sandstone at different cyclic stress stages were analyzed in detail. By combining the mathematical statistics, fluctuation coefficients of the residual strain and energy dissipation, and correlation coefficients of axial/radial residual strain and energy dissipation were defined to describe the process. It was determined that these newly defined physical variables were closely related to the elastic-plastic state (or instability failure state) of the rock.

Introduction

Granular materials such as soils, rocks, and other granular-filling materials, frequently exhibit nonlinear behavior, including noncontinuity [1], anisotropy [2], non-complete elasticity [3], slow dynamic effects [4, 5], stick-slip [6], and dynamic wave hysteresis [7, 8]. This study focuses on the instability of the deformations and dissipation energies during cyclic loading and unloading processes caused by the noncontinuity and anisotropy of sandstone. These properties are clearly reflected in the nonlinear deformation processes of rocks subjected to cyclic loading [9]. When these processes occur in natural environments, geotechnical engineering construction, and long-term operation, rock and soil masses are often subjected to cyclic or even dynamic loading [10–15]. Cyclic loading causes a complex and sudden nonlinear deformation as well as nonuniform damage to the rock [16, 17]. There are some deviations in the predictions of deformation and failure for nonlinear rock. This is because in the traditional method, rock is regarded as a linear elastic material. Therefore, the study of the nonlinear behavior of rock under cyclic loading is necessary for a better understanding of the damage and failure mechanisms of rock.

In regard to the nonlinear behavior of rock under cyclic loading, many scholars have conducted experiments with different rock types [9–27]. For example, Li et al. [9] established a damage model based on the nonlinear behavior of rocks, and considered the initial damage from fractured rocks from the perspective of energy dissipation. Tong et al. [18] used a Split-Hopkinson pressure bar (SHPB) system to study the nonlinear dynamics of sandstone under different external confining pressures, by exploring the higher harmonics generated by impact loading. David et al. [19] corrected Walsh's model for the effects of cracks on the uniaxial stress-strain curves of rock, and provided a micromechanical explanation for nonlinear and hysteretic stress-strain behavior. Bagde et al. [20, 21] conducted uniaxial cyclic loading tests on sandstone under different amplitudes and frequencies. Effects of the strain, amplitude, and frequency of cyclic loading on the fatigue and nonlinear characteristics of sandstone were studied. Araei et al. [22] experimentally investigated the influence of the initial stress state and loading rate on the nonlinear and hysteretic stress-strain curves of rock under uniaxial cyclic loading. The main focus in the above studies regarding nonlinear characteristics under cyclic loads is hysteresis. However, the volatility of the physical properties of rock under cyclic loading has rarely been studied, especially the fluctuations of residual strain and dissipated energy, and the correlations of axial/radial residual strains and energy dissipations in each cycle under tiered cyclic loading. In addition, the effect of cyclic loading on a rock specimen is based on the cumulative effects during each cycle [23]. The residual deformation and dissipated energy can reflect the fatigue damage process during cyclic loading. Thus, a study of the fluctuations of axial/radial residual deformations and dissipated energy under cyclic loading and their correlations will contribute to understanding the failure mechanism of rock under cyclic fatigue, and to predicting the failure instability of rock.

As rocks are composed of many intimate mineral grains forming a solid frame, the presence of intercrystalline cracks and microstructure boundaries is unavoidable [28]. It is this granular microstructure that causes the fluctuating and nonlinear responses of the rock under external stress [29]. This fluctuating and nonlinear behavior of rock is well known by rock mechanics researchers. In this work, the deformation properties and energy dissipation characteristics of saturated sandstone were experimentally studied under tiered cyclic loading. As rock is a natural heterogeneous material, the residual deformation and dissipated energy show evident fluctuations during the cyclic loading process. The fluctuations of the rock deformation and dissipative energy can reflect the unstable state of the rock during constant-amplitude cyclic loading. Therefore, fluctuation coefficients for residual strain and energy dissipation, correlation coefficients for axial/radial residual strains and energy dissipations were newly defined to describe this process. Finally, the newly defined physical variables were used to identify the elastic plastic state (instability failure state) of the rock. The specific purpose of this study is to evaluate the stability and nonlinear mechanical behavior of an underwater rock mass in the Three Gorges Reservoir area under a cyclic load.

Experiment setup

Experimental apparatus

This experiment was implemented using a RLW-2000M microcomputer controlled coal rock rheometer from Chongqing University, which was produced by Changchun City Chaoyang Test System Co., Ltd. The apparatus was mainly composed of a computer control system, tri-axial pressure chamber, axial loading system, confining pressure system, pore water pressure system, and temperature control. The control system adopted an EDC (entire digital control) system imported by the DoLI company of Germany. The system was divided into three independent closed-loop control systems, including systems for axial pressure, confining pressure,

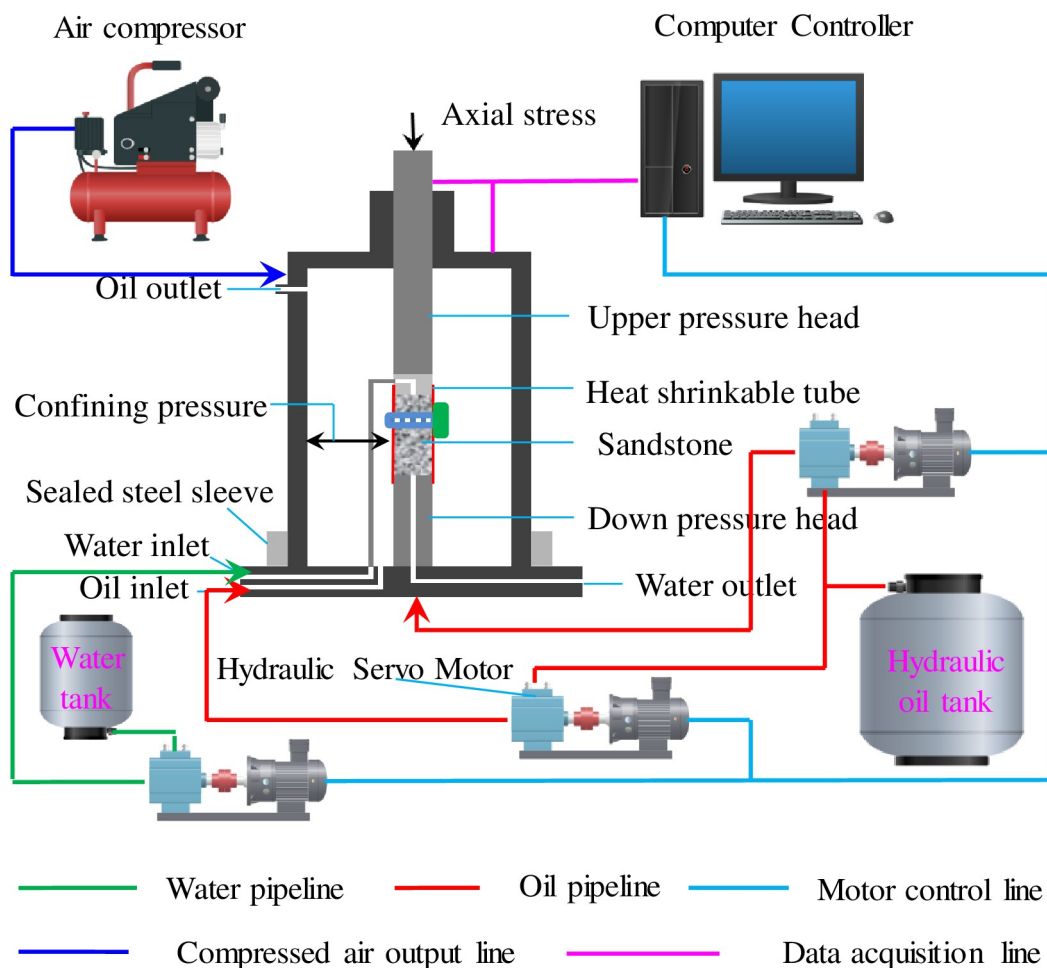


Fig 1. RLW-2000M triaxial creep testing machine.

<https://doi.org/10.1371/journal.pone.0236335.g001>

and pore pressure. The loading system was a servo motor and ball screw loading system, which can automatically perform the uniaxial compressive strength test, triaxial compressive strength test, cyclic loading test, and rheological test on the rock. It has a maximum axial load of 2000 kN, effective force measurement range of 10–2000 kN, maximum confining pressure of 60 MPa, confining pressure measurement accuracy of $\pm 1\%$, and maximum pore water pressure of 40 MPa. A diagram of the instrument used for experiment is shown in Fig 1.

Preparation of sandstone samples

The sandstone specimens used in the test were taken from outcrops in the Chongqing District [30], in the Sichuan Basin in the southwest of China (see Fig 2), located in the Three Gorges Reservoir area. The sample collection area in this study is not owned by any company and belongs to public natural resources. The experimental equipment is owned by Chongqing University where the author works; hence, permits were not required. The purpose of this experiment was to evaluate the stability of the underwater rock mass in the Three Gorges Reservoir area under cyclic loading. Therefore, saturated sandstone was selected as the experimental specimen. The study of the mechanical properties of saturated sandstone under repeated engineering disturbances has an important role in ensuring the stability of the rock mass in the Three Gorges Reservoir area. Sandstones are terrigenous fine-grained clastic sedimentary

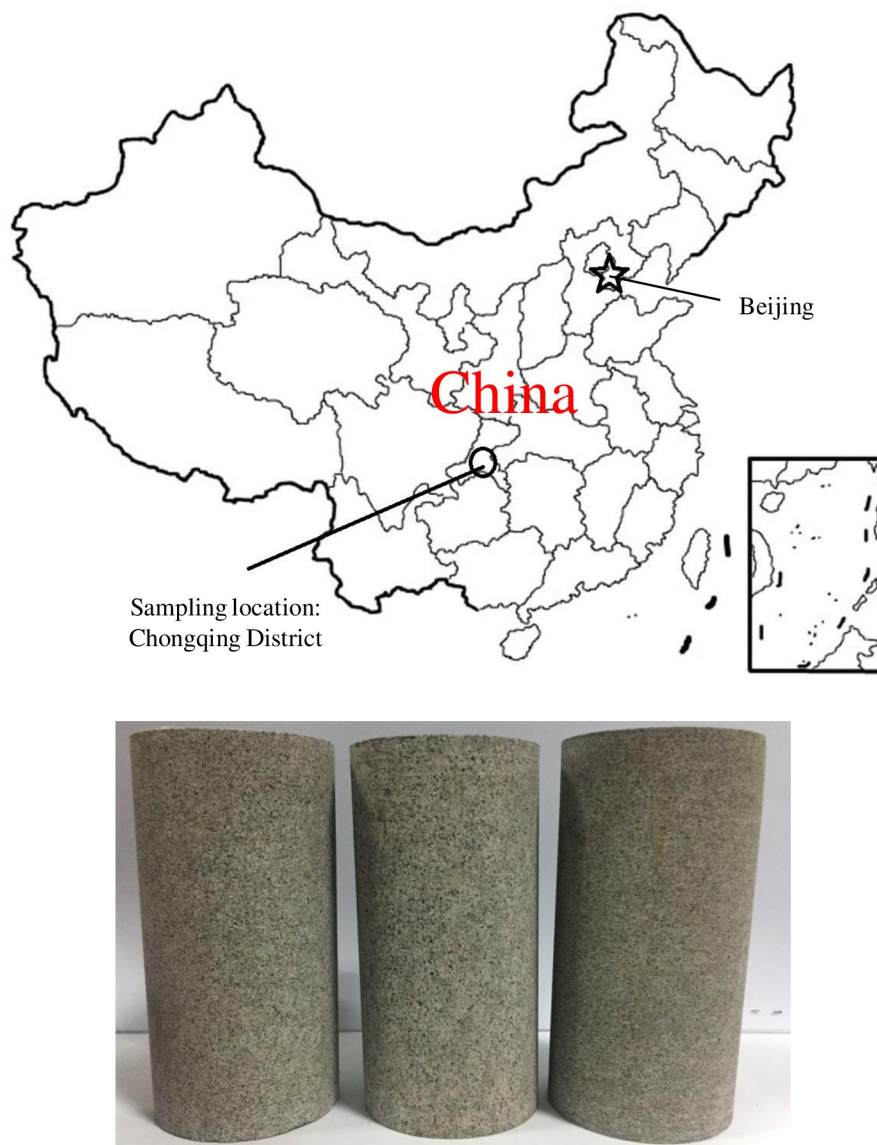


Fig 2. The sandstone samples and sample location.

<https://doi.org/10.1371/journal.pone.0236335.g002>

rocks, and are mainly composed of quartz, feldspar and muscovite. The internal structure of sandstone is made up of fine to medium size sand particles with pore structures between the sand particles, cemented mainly by siliceous and carbonate material. According to the ISRM, the samples were processed by wet processing into standard samples with 50 mm in diameter and 100 mm in height. In addition, the sample cross section was cut and polished such that the end face evenness was controlled to within 0.02 mm [31]. The basic physical parameters of the sandstone are listed in Table 1. Fig 3 shows the sandstone internal particle micro-structure, obtained via scanning electron microscopy [32]. As the effects of the pore water pressure were

Table 1. Basic physical parameters of sandstone.

Natural moisture content (%)	Density (g/cm ³)	Modulus of elasticity (GPa)	Poisson ratio	Cohesive force (MPa)	Internal friction angle (°)
3.8	2.45	13.8	0.27	14.5	42

<https://doi.org/10.1371/journal.pone.0236335.t001>

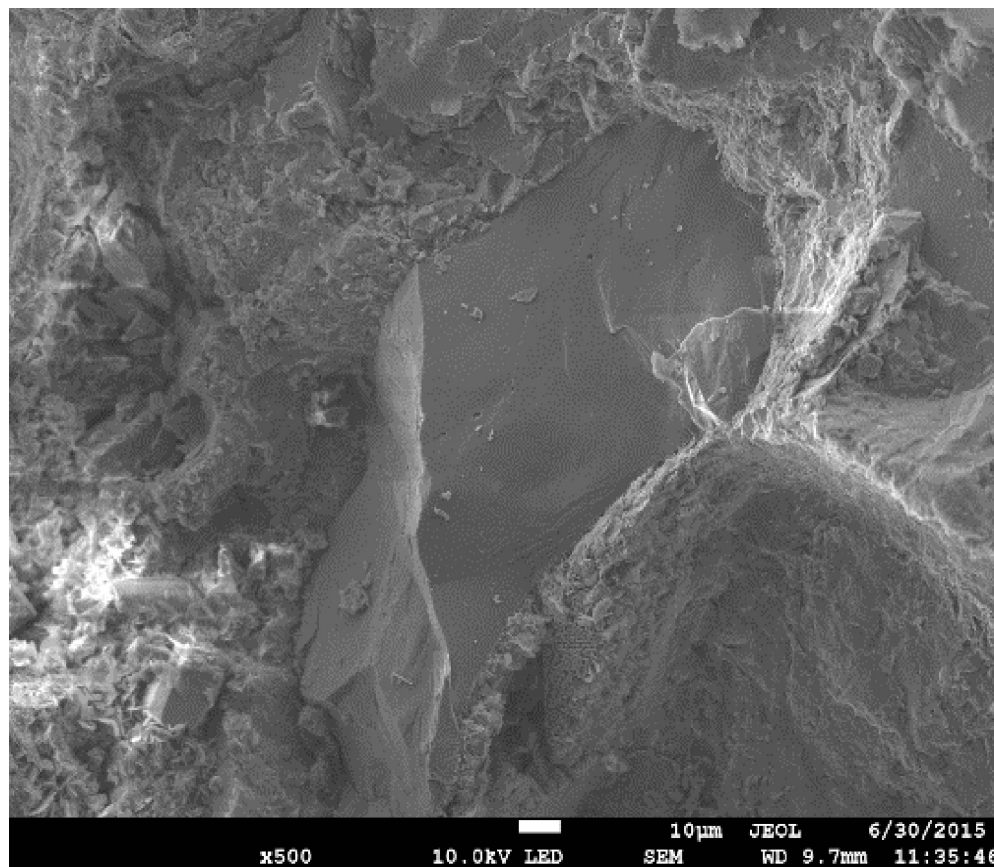


Fig 3. Sandstone internal particle micro-structure scanned by SEM [32].

<https://doi.org/10.1371/journal.pone.0236335.g003>

considered in the experiment, it was necessary to prepare a saturated sandstone specimen. A water-saturated apparatus was used to prepare the saturated specimen, as shown in Fig 4. Jiang et al. [33] can be referred to for specific water saturation steps.

Experiment scheme

In this experiment, saturated sandstone was initially placed into the triaxial pressure chamber. Thereafter, the triaxial pressure chamber was filled with hydraulic oil to apply the confining pressure. After making contact with the axial indenter, an axial force was applied to 20 kN at a speed of 0.1 kN/s. The confining pressure was applied to a hydrostatic pressure of 10 MPa at a speed of 0.05 MPa/s, and the water pressure was loaded to a target value (3 and 6 MPa) at a speed of 0.05 MPa/s. The confining and water pressures were kept constant, and the axial stress continued to be loaded to 70 kN. After the deformation displacement and stability state, the axial stress entered a stage of tiered cyclic loading; the path for the axial stress tiered cyclic loading is illustrated in Fig 5(A). Each cycle stage was numbered, and the final cycle stage was called the failure stage. The cyclic frequency was set to 0.02 Hz, and the cycle number was set to 140 times per cycle stage. The stress amplitude was set to 50 kN for each cycle stage. The axial stress was set to an increment of 20 kN per stage, and continuous cyclic loading was conducted until failure of the sandstone specimen. To smooth the peak and valley of the stress-strain curve from the cyclic loading, a sinusoidal wave was used as the loading waveform in this experiment, as shown in Fig 5(B).

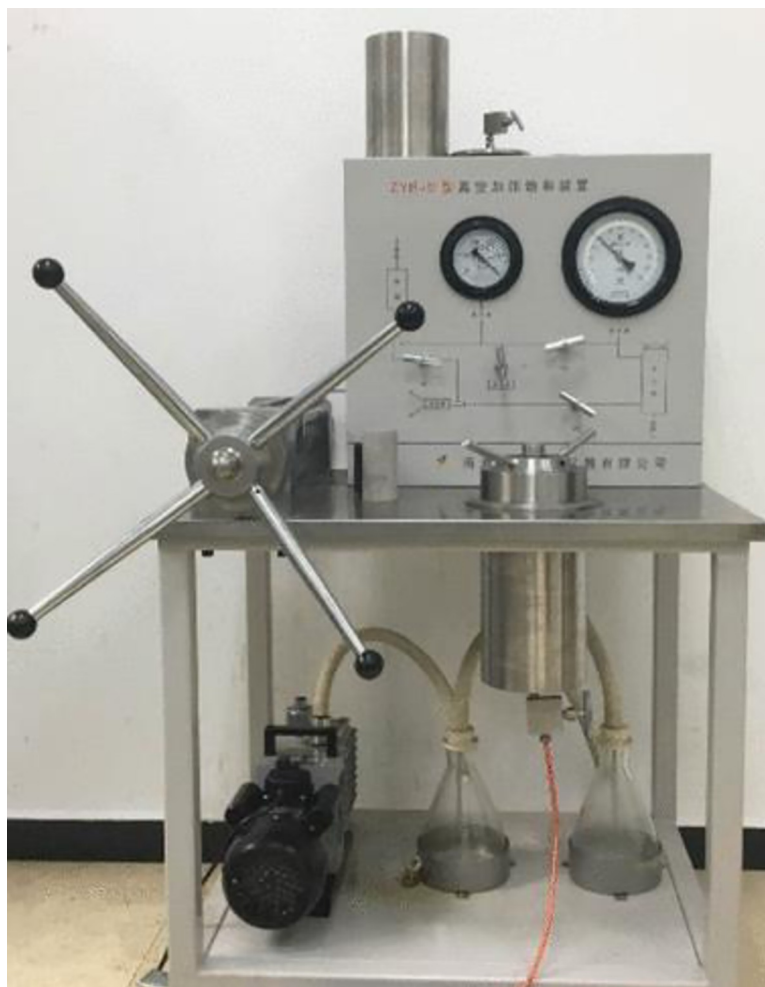


Fig 4. Water-saturated apparatus [33].

<https://doi.org/10.1371/journal.pone.0236335.g004>

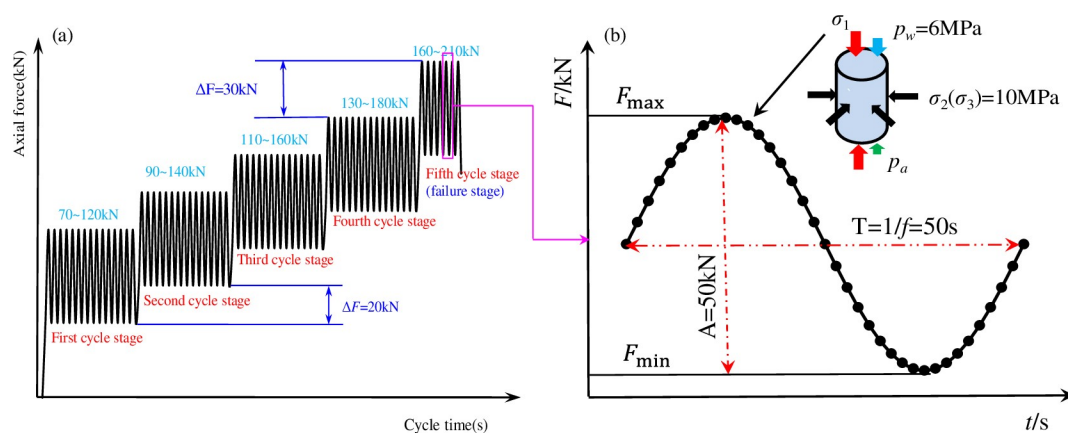


Fig 5. Schematic diagram of tiered cyclic loading and Sketch of sine wave loading (water pressure 6MPa).

<https://doi.org/10.1371/journal.pone.0236335.g005>

Table 2. Basic experimental data from sandstone sample.

Sample	Cycle stage	$\xi_1(10^{-7})$	$\xi_3(10^{-7})$	χ_1	χ_3	ρ_p	ρ_d
SS-1 (water pressure 3 MPa)	1th	0.589	0.1721	0.0143	0.0395	-0.808	-0.750
	2th	0.239	0.1455	0.0075	0.0152	-0.925	-0.948
	3th	0.485	0.6401	0.0254	0.0395	-0.931	-0.958
	4th	0.766	0.9673	0.0389	0.0452	-0.445	-0.574
	5th	18.557	16.270	0.1291	0.1554	-0.433	-0.521
SS-2 (water pressure 6 MPa)	1th	0.569	0.1074	0.120	0.300	-0.873	-0.896
	2th	0.493	0.0882	0.024	0.035	-0.923	-0.902
	3th	2.734	0.1658	0.145	0.065	-0.956	-0.965
	4th	3.682	0.2256	0.523	0.153	-0.930	-0.925

ξ_1 and ξ_3 are the fluctuation coefficients of $\Delta\epsilon_{p1}$ and $\Delta\epsilon_{p3}$, respectively; χ_1 and χ_3 are the fluctuation coefficients of ΔU_{d1} and ΔU_{d3} , respectively; ρ_p is the correlation coefficient of $\Delta\epsilon_{p1}^{ij}$ and $\Delta\epsilon_{p3}^{ij}$; ρ_d is the correlation coefficient of ΔU_{d1}^{ij} and ΔU_{d3}^{ij} .

<https://doi.org/10.1371/journal.pone.0236335.t002>

Experimental results and analysis

In this experiment, the tiered cyclic loading tests were carried out on two saturated sandstone specimens (SS-1 and SS-2) under different water pressures (3 MPa and 6 MPa, respectively). The characteristics of the axial/radial deformations and energy dissipations were compared and analyzed under different cycle stages and different water pressures. By analyzing these value and their correlations, the rock mass deformation instability and damage could be predicted. Table 2 provides the basic experimental data from SS-1 and SS-2. (Note: SS is the abbreviation for saturated sandstone)

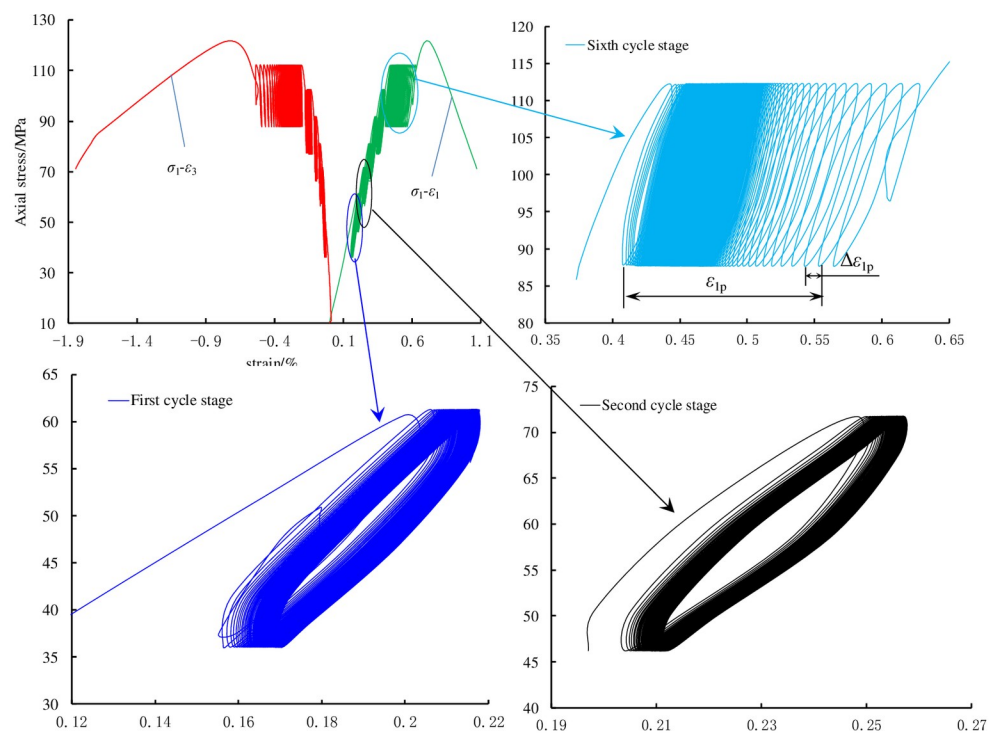
Characteristics of residual strain in sandstone under tiered cyclic loading

The full stress-strain curves of the two saturated sandstone specimens under tiered cyclic loading are illustrated in Fig 6. The stress-strain curves of the sandstone specimens under different water pressures were similar during cyclic loading. A large amount of plastic deformation was produced in each sandstone specimen at each cycle stage. With an increase of the cyclic stage, the cyclic stress-strain curve showed characteristics of three different stages, i.e., sparse, then dense, and later sparse again. Owing to the existence of micro-pores, cracks, and soft interfaces in the sandstone, the deformation of the sandstone at the initial cyclic stage was large. With the increase of stress, the sandstone was gradually compacted and the plastic deformation decreased. When the cyclic stress exceeded the fatigue threshold stress of the sandstone, plastic deformation increased.

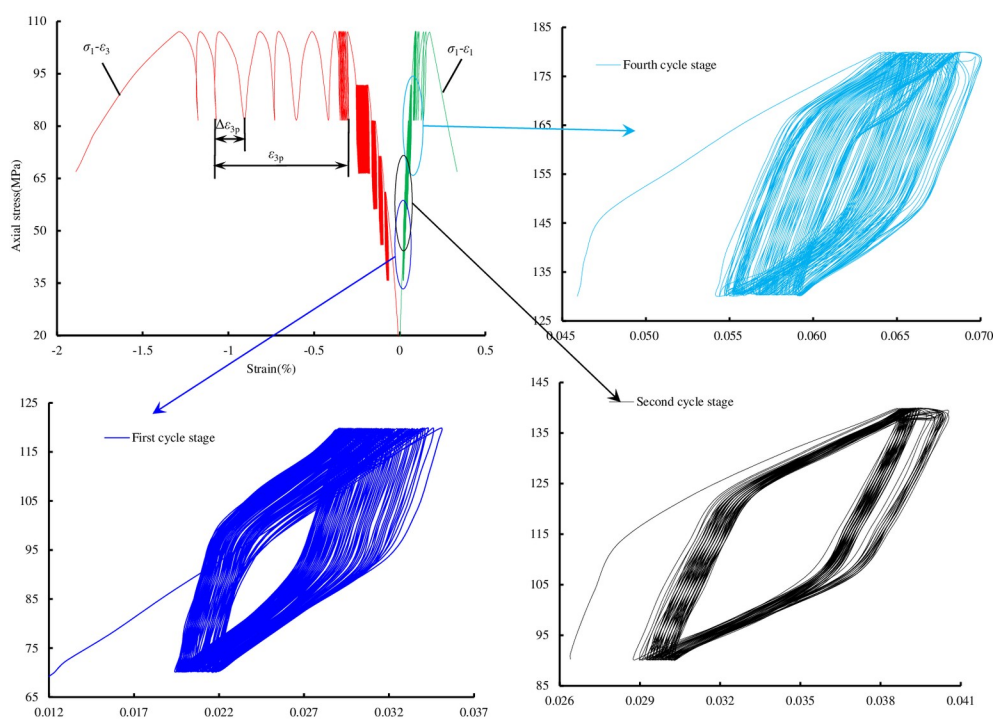
To analyze the residual strain of the sandstone during the cyclic loading process more precisely, the formulas for calculating the accumulated residual strain and relative residual strain at different cycle stages were defined as follows

$$\begin{cases} \epsilon_p^{ij} = \epsilon^{ij} - \epsilon^{i0} \\ \Delta\epsilon_p^{ij} = \epsilon^{ij} - \epsilon^{i(j-1)} \end{cases} \quad (1)$$

where ϵ_p^{ij} is the accumulated residual strain at j th cycle in the i th cycle stage; it includes the accumulated axial residual strain (ϵ_{p1}^{ij}), and the accumulated radial residual strain (ϵ_{p3}^{ij}). $\Delta\epsilon_p^{ij}$ is the relative residual strain at the j th cycle in the i th cycle stage, and also includes the relative axial residual strain ($\Delta\epsilon_{p1}^{ij}$) and relative radial residual strain ($\Delta\epsilon_{p3}^{ij}$).



(a)SS-1



(b)SS-2

Fig 6. Full stress-strain curves and local enlarged diagrams of sandstone under multilevel cyclic loading.

<https://doi.org/10.1371/journal.pone.0236335.g006>

The change in ε_p^{ij} under different cyclic stress level

The values of ε_{p1}^{ij} and ε_{p3}^{ij} can be calculated using Eq (1), and the results for SS-1 and SS-2 are shown in Fig 7. It can be seen that the changes in the accumulated residual strain under different water pressures are similar. However, the smaller the water pressure, the smoother the residual strain curve and the smaller the deformation fluctuation. The accumulated residual strain increased with the increase of the cyclic stress (or stage), but it showed different changes in each cycle stage with the increasing cycle number.

1. The change in ε_{p1}^{ij} : When the cyclic stress is in the elastic stage (i.e., in the first few cycle stages), ε_{p1}^{ij} initially increases rapidly, then gradually, and finally becomes stable; when the cyclic stress is in the yield stage (i.e., in the several cycle stages before destruction), ε_{p1}^{ij} shows a large increase and fluctuates greatly, and there is an evident inflection point (or strain-softening point), as depicted in Fig 7. In the cyclic destruction stage, the change trend of ε_{p1}^{ij} shows an evident acceleration deceleration acceleration process. It increases sharply, and the portion near failure increases linearly.
2. The change in ε_{p3}^{ij} : The absolute value of ε_{p3}^{ij} has the same change as that of ε_{p1}^{ij} . The evident inflection point also appears in the same cycle stage. As the stresses increase gradually,

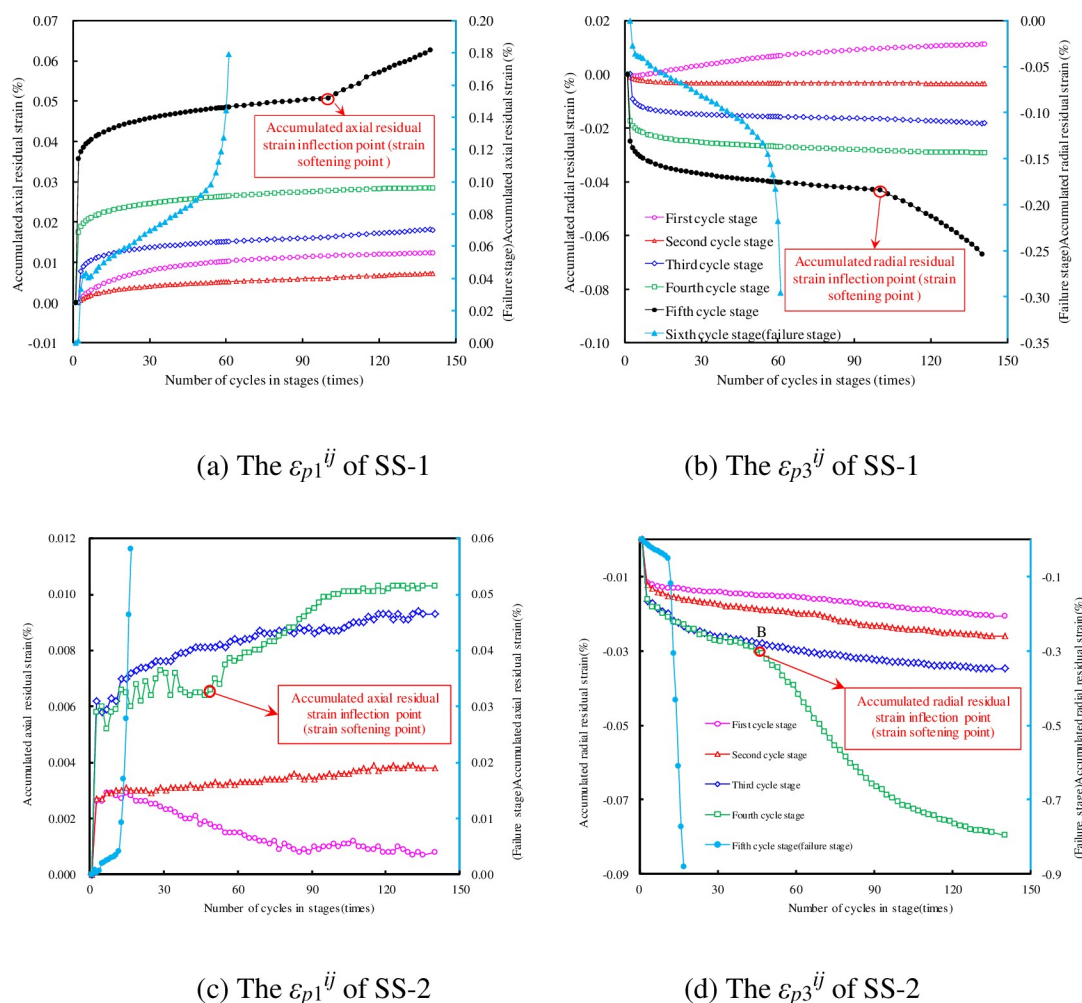


Fig 7. Accumulated residual strain curves at different cycle stages.

<https://doi.org/10.1371/journal.pone.0236335.g007>

when the stress reaches the fatigue threshold stress for sandstone, the strain of the sandstone under cyclic loading increases sharply.

The change in $\Delta\epsilon_p^{ij}$ under different cyclic stress level

The values of $\Delta\epsilon_{p1}^{ij}$ and $\Delta\epsilon_{p3}^{ij}$ at each cycle stage can be calculated using Eq (1), as shown in Fig 8. To clearly observe the relative residual strain of SS-2 in each cycle stage, the $\Delta\epsilon_p^{ij}$ curve for the first 20 cycles in each cycle stage is enlarged. The change in $\Delta\epsilon_p^{ij}$ in the sandstone can be divided into two stages.

1. Before failure stage: In the first 4th (or 5th) cycle stages, and with the increase of cycle number, the values of $\Delta\epsilon_{p1}^{ij}$ and the absolute value of $\Delta\epsilon_{p3}^{ij}$ are larger in the initial cycles, and then gradually approach the cyclic stability line (i.e., the 0 line). The relative residual strain fluctuates in the vicinity of the 0 line, even infinitely close to 0. This indicates that the initial residual deformation at each stage is large, then decreases gradually, before finally reaching nearly 0.

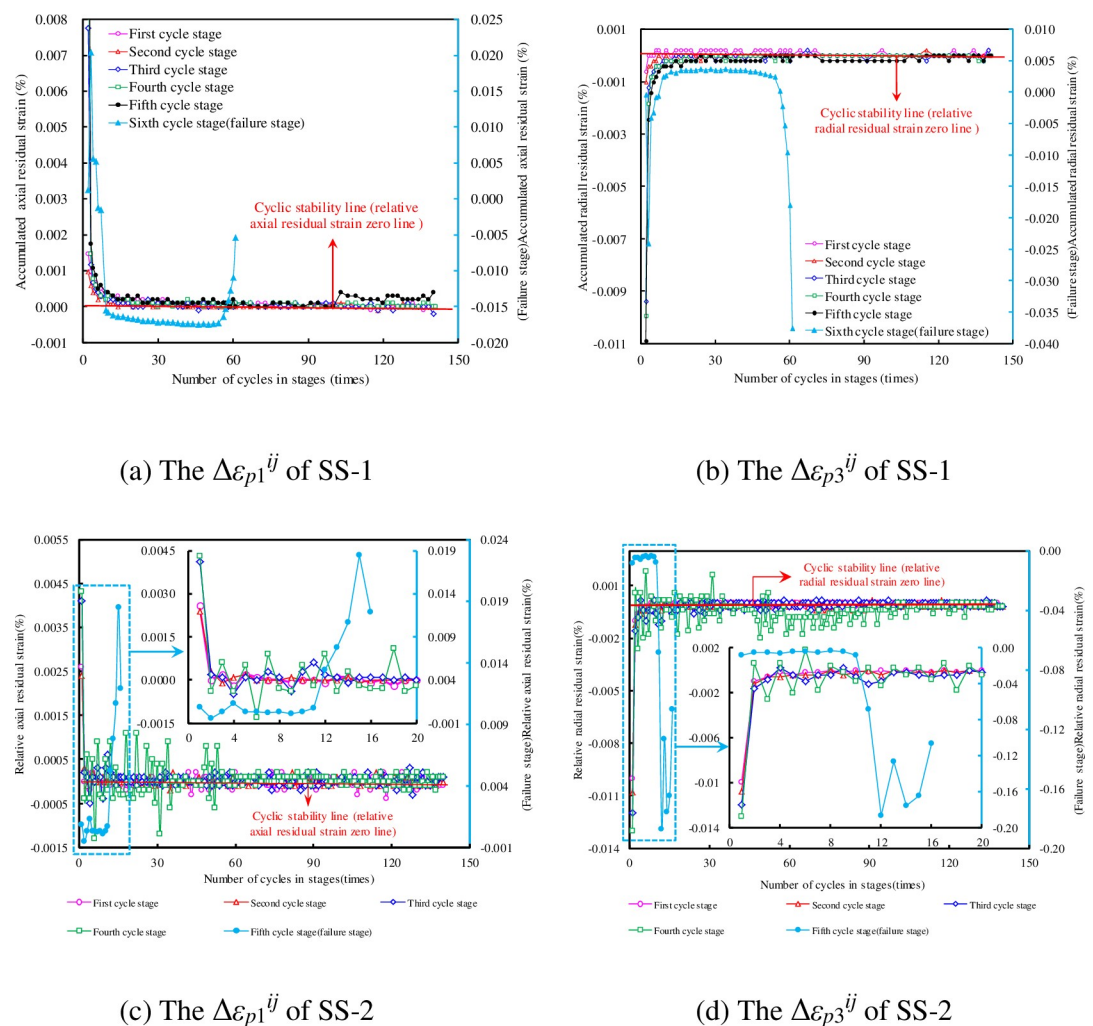


Fig 8. Relative residual strain curve at different cycle stages.

<https://doi.org/10.1371/journal.pone.0236335.g008>

2. Failure stage: In the 5th (or 6th) cycle stage, with the increase of cycle number, the values of $\Delta\epsilon_{p1}^{ij}$ and absolute value of $\Delta\epsilon_{p3}^{ij}$ begin to increase slowly, and then increases sharply when the samples are near failure.

Characteristic dissipation energy in sandstone under tiered cyclic loading

In addition to the residual strains, plastic hysteresis loops were also produced in the cyclic stress-strain curves of the sandstone. The residual strain can only reflect the plastic deformation at the unloading point; in contrast, the area of the plastic hysteresis loop is a process quantity which can reflect the deformation of the sandstone during the entire loading-unloading process. The physical implication of the hysteresis loop area is the energy dissipation of the rock during the process of a single loading and unloading [12, 34]. Energy dissipation is an essential property of rock failure and a common measure for analyzing the failure process [24, 35–37]. Therefore, it is necessary to conduct a detailed analysis of the energy dissipation under tiered cyclic loading.

During the loading process, rock deformations occur owing to the effects of external forces, and the total energy (U) input from an external force to a rock sample is mainly stored as an elastic potential energy (U_e) accumulated in the rock mass. A small part of the energy (U_d) is lost in various forms of damage dissipation. The elastic potential energy is released when unloading. In this study, this energy was approximately equal to the negative work U_r done by the external forces during unloading [12, 34] as follows:

$$U = U_e + U_d \approx U_r + U_d = \int \sigma_1^+ d\epsilon_1^+ + 2 \int \sigma_3^+ d\epsilon_3^+ \quad (2)$$

$$U_r = \int \sigma_1^- d\epsilon_1^- + 2 \int \sigma_3^- d\epsilon_3^- \quad (3)$$

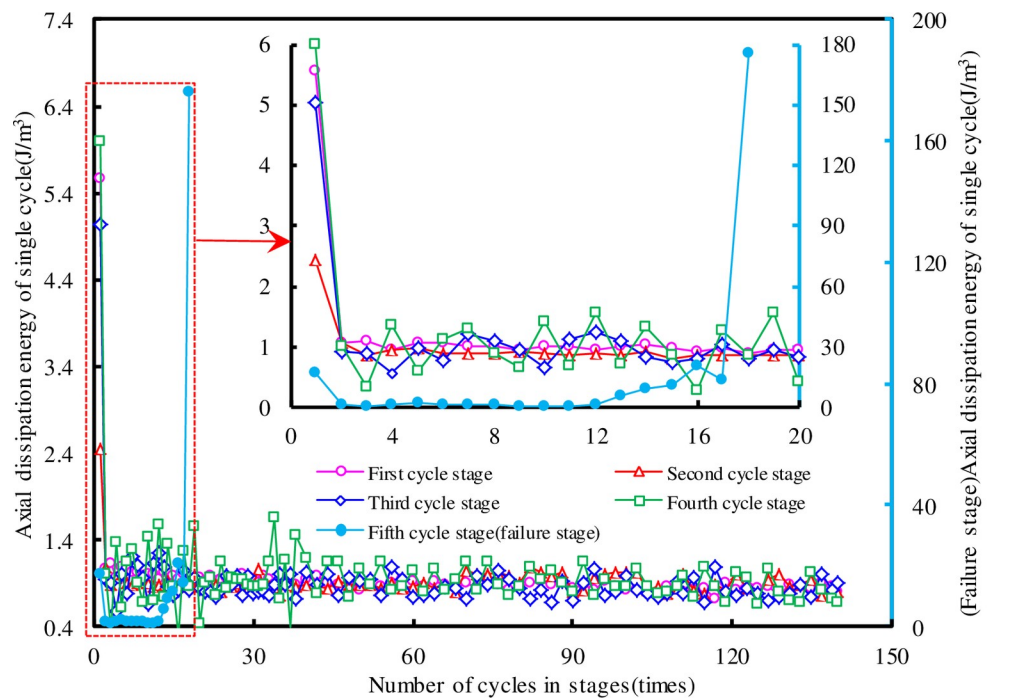
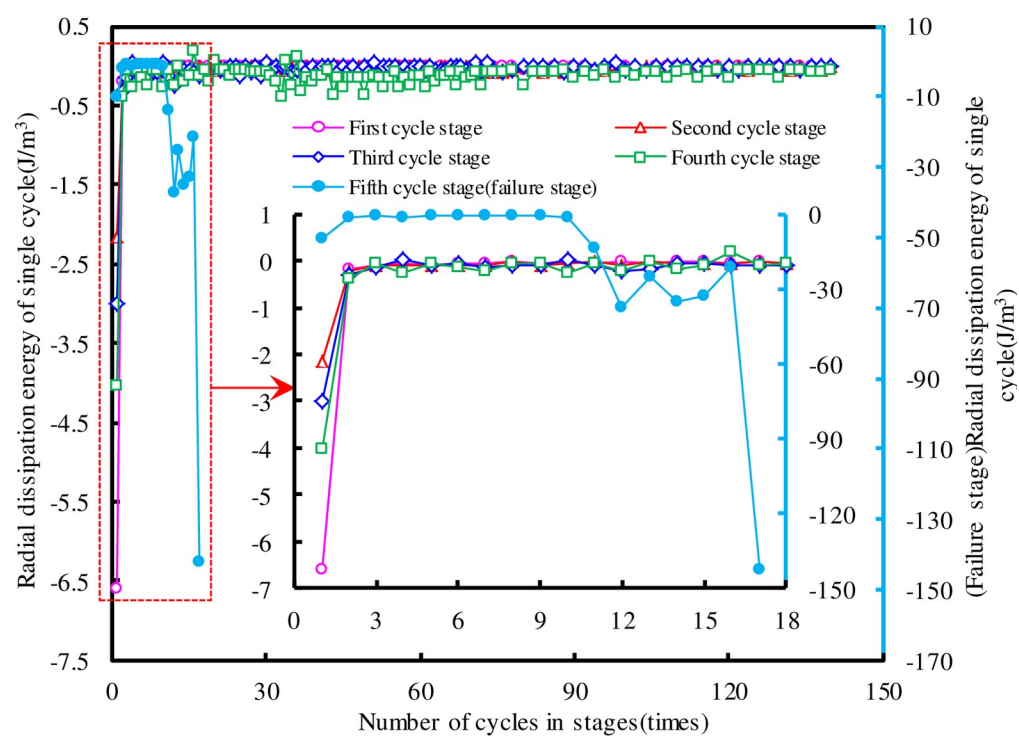
The area of a plastic hysteresis loop represents the single cycle dissipation energy, including the axial dissipation energy and radial dissipation energy [35]. In combination with the definition of a differential, the axial dissipation energy and radial dissipation energy can be calculated as follows [12, 34–37]:

$$U_d = U - U_r = \left(\int \sigma_1^+ d\epsilon_1^+ - \int \sigma_1^- d\epsilon_1^- \right) + 2 \left(\int \sigma_3^+ d\epsilon_3^+ - \int \sigma_3^- d\epsilon_3^- \right) = U_{d1} + U_{d3} \quad (4)$$

$$\int \sigma d\epsilon = \sum_{i=1}^n \frac{1}{2} (\sigma^i + \sigma^{i-1}) (\epsilon^i - \epsilon^{i-1}) \quad (5)$$

where U_{d1} and U_{d3} are the axial and radial dissipation energy, respectively. σ_1^+ , ϵ_1^+ , σ_1^- , and ϵ_1^- are the stress and strain values at each point of the axial stress-strain curve in the loading and unloading stages, respectively, and σ_3 is radial stress. ϵ_3^+ and ϵ_3^- are the radial strain at loading and unloading stages, respectively. ΔU_d indicates the single cycle dissipated energy.

As the dissipative energy laws of the two sandstone specimens are similar (the smaller the water pressure, the smoother the dissipation energy curve.), only the dissipative energy evolution law of SS-2 was analyzed in detail. The changes of ΔU_{d1} and ΔU_{d3} in SS-2 are shown in Fig 9. It can be seen that ΔU_{d3} is negative, indicating that the specimen do work to hydraulic oil in the radial direction during cycle loading. The curve of ΔU_d for the first 20 cycles at each cycle stage is also enlarged. There were similarities between the variation trends of ΔU_d and $\Delta\epsilon_p$. The change in ΔU_d can also be divided into two stages (i.e., a pre-destruction stage and destruction stage).

(a) ΔU_{d1} (b) ΔU_{d3} **Fig 9. The curve of ΔU_d in the SS-2 at different cycle stages.**

<https://doi.org/10.1371/journal.pone.0236335.g009>

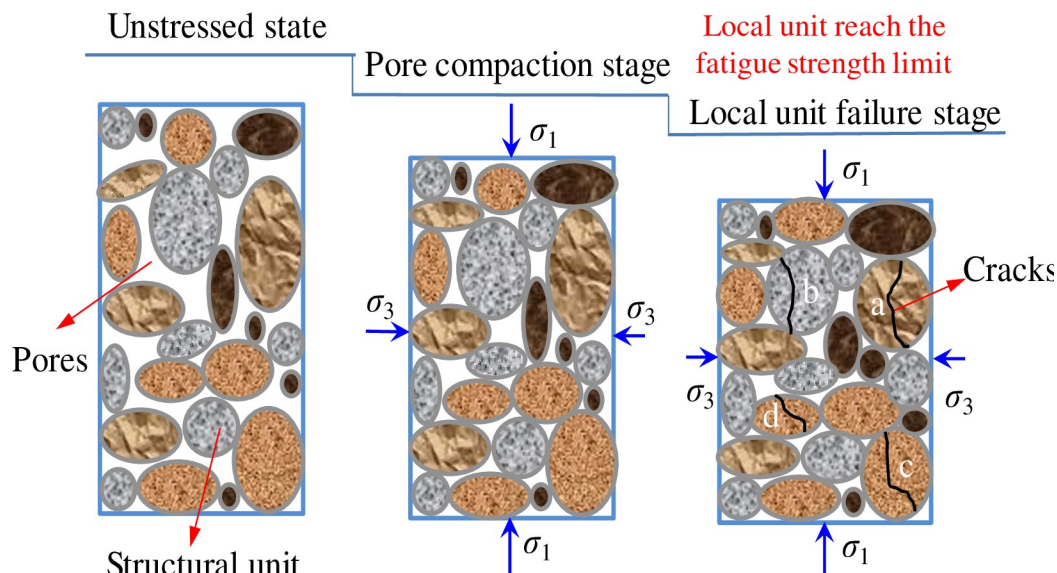


Fig 10. Schematic diagram of deformation and failure of sandstone structural units under external force.

<https://doi.org/10.1371/journal.pone.0236335.g010>

Fluctuations of $\Delta\epsilon_p$ and ΔU_d under tiered cyclic loading

From Figs 8 and 9, it is observed that the curves of ΔU_d and $\Delta\epsilon_p$ show some fluctuation in each cycle stage before the destruction stage; this phenomenon has also been found in other studies [38–42]. There are many explanations for this phenomenon, but it is generally accepted that a rock mass is composed of micro-structural elements (see Fig 10). Each micro-structural element has fatigue strength limit. When the cyclic stress reaches the failure strength limit of each micro-structural element, local failure occurs and the residual deformation of rock suddenly increases [9, 23]. However, other researchers believe that sandstone subjected to cyclic stress displays complex stress-strain characteristics of nonlinearity and hysteresis, owing mainly to nonlinear deformations and the frictional sliding of grain contacts [40–42]. The phenomenon of unstable deformation (or unstable damage) of sandstone exactly reflects that sandstone is a natural product of heterogeneity and anisotropy [43, 44]. The stability of the rock can be predicted by analyzing the fluctuations of the deformation and dissipation energy.

By applying the theory of variance in mathematical statistics, the fluctuation coefficient of $\Delta\epsilon_p$ was defined as the variance of $\Delta\epsilon_p$ in each cycle stage before failure. The fluctuation coefficient of $\Delta\epsilon_p$ was calculated as follows:

$$E(\Delta\epsilon_p^{ij}) = \sum_{j=1}^{140} (\Delta\epsilon_p^{ij}) / 140 \quad (6)$$

$$\xi = D(\Delta\epsilon_p^{ij}) = E\{[\Delta\epsilon_p^{ij} - E(\Delta\epsilon_p^{ij})]^2\} \quad (7)$$

where $E(\Delta\epsilon_p^{ij})$ is the expected value of $\Delta\epsilon_p$ in the i th cycle stage before failure. ξ is the variance of $\Delta\epsilon_p$ in the i th cycle stage before failure. ξ_1 and ξ_3 are the fluctuation coefficients of $\Delta\epsilon_{p1}$ and $\Delta\epsilon_{p3}$, respectively.

The values of ξ_1 and ξ_3 are illustrated in Fig 11; they exhibit the same trend with the increase of cycle stage, i.e., both initially decrease and then increase. In the initial cycle stage, owing to the large number of micro-pores, cracks, and weak zones in the original rock mass, unstable deformation easily occurs under stress. With an increase of cyclic stress, the pore fracture is

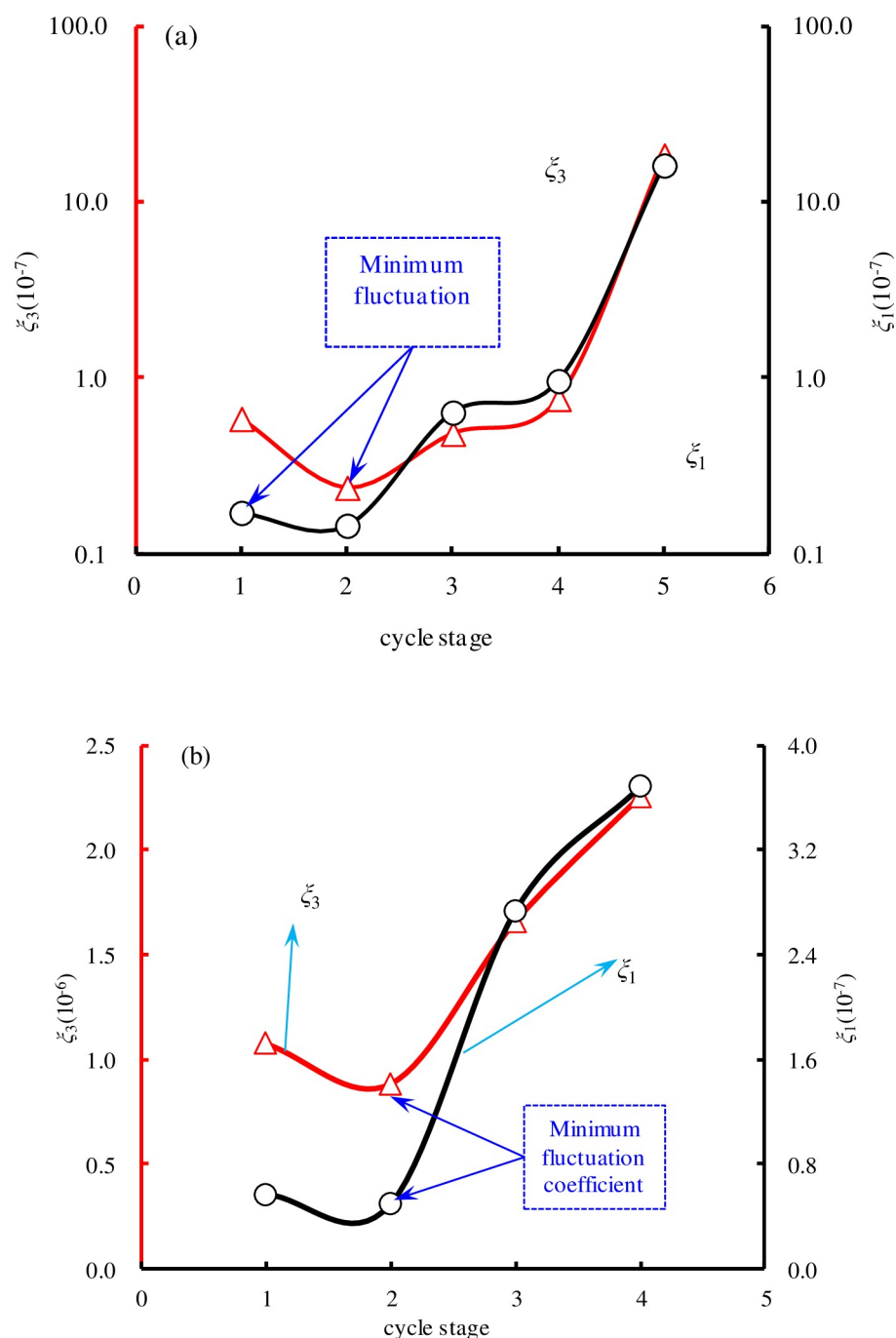


Fig 11. Fluctuation coefficient curve of relative residual strain: (a) SS-1; (b) SS-2.

<https://doi.org/10.1371/journal.pone.0236335.g011>

gradually compacted, and the rock mass tends to be elastic. Thus, the fluctuation of $\Delta\epsilon_p$ decreased in second cycle stage, and the variance of $\Delta\epsilon_p$ was close to 0. As the cyclic stress continued to increase, new pores and fissures gradually expanded, and local failures resulted in unstable deformations. The fluctuation of $\Delta\epsilon_p$ increased rapidly, and the deformation of the rock mass became increasingly unstable. This shows that the deformation has great fluctuations when the rock mass tends to instability. The characteristics of $\Delta\epsilon_p$ can be used to predict whether rock mass failure will occur during cyclic loading.

In the same way, the fluctuation coefficient of ΔU_d was calculated as follows:

$$E(\Delta U_d^{ij}) = \sum_{j=1}^{140} (\Delta U_d^{ij}) / 140 \quad (8)$$

$$\chi = D(\Delta U_d^{ij}) = E\{[\Delta U_d^{ij} - E(\Delta U_d^{ij})]^2\} \quad (9)$$

where $E(\Delta U_d^{ij})$ is the expected value of the single cycle energy dissipation in the i th cycle stage before failure. χ is variance value of the single cycle energy dissipation in the i th cycle stage before failure. χ_1 and χ_3 are the fluctuation coefficients of ΔU_{d1} and ΔU_{d3} , respectively.

As shown in Fig 12, the change trend of χ is the same as the change trend of ξ , but χ is disproportionate to ξ . This shows that there is a certain relationship (but not a linear relationship) between the residual strain and energy dissipation under cyclic loading. χ_1 and χ_3 show the same trend with increasing cycle stage, i.e., initial decrease and then increase. There was some instability in the energy dissipation at the initial stage and near the destruction stage. The characteristics of ΔU_d can also be used as a precursor for predicting rock damage.

Correlation coefficients of axial/radial residual strains and energy dissipations

From Figs 11 and 12, it can be seen that there is some correlation between the axial and radial residual strains (or energy dissipations); this indicates that the axial and radial physical variables are interrelated, and interact with each other. The relationship between axial and radial strains is most commonly expressed by Poisson's ratio. For perfectly elastic materials, the Poisson's ratio is a constant, and shows that the relationship between the axial and radial strains is linear. For sandstone, the Poisson's ratio varied under stress loading, indicating that the relationship between the axial and radial strains is nonlinear. To observe correlation strength between the axial and radial relative residual strains, the correlation coefficients of $\Delta \epsilon_{p1}$ and $\Delta \epsilon_{p3}$ are defined as follows:

$$\text{Cov}(\Delta \epsilon_{p1}^{ij}, \Delta \epsilon_{p3}^{ij}) = E\{[\Delta \epsilon_{p1}^{ij} - E(\Delta \epsilon_{p1}^{ij})][\Delta \epsilon_{p3}^{ij} - E(\Delta \epsilon_{p3}^{ij})]\} \quad (10)$$

$$\rho_p = \text{Cov}(\Delta \epsilon_{p1}^{ij}, \Delta \epsilon_{p3}^{ij}) / \sqrt{\xi_1 \xi_3} \quad (11)$$

where $\text{Cov}(\Delta \epsilon_{p1}^{ij}, \Delta \epsilon_{p3}^{ij})$ is the covariance of $\Delta \epsilon_{p1}^{ij}$ and $\Delta \epsilon_{p3}^{ij}$; ρ_p is the correlation coefficient of $\Delta \epsilon_{p1}^{ij}$ and $\Delta \epsilon_{p3}^{ij}$, and can reflect the correlation strength between the axial residual strain and radial residual strain in each cycle stage.

In the same way, the correlation coefficients of the single cycle axial and radial energy dissipations are defined as follows:

$$\text{Cov}(\Delta U_{d1}^{ij}, \Delta U_{d3}^{ij}) = E\{[\Delta U_{d1}^{ij} - E(\Delta U_{d1}^{ij})][\Delta U_{d3}^{ij} - E(\Delta U_{d3}^{ij})]\} \quad (12)$$

$$\rho_d = \text{Cov}(\Delta U_{d1}^{ij}, \Delta U_{d3}^{ij}) / \sqrt{\chi_1 \chi_3} \quad (13)$$

where $\text{Cov}(\Delta U_{d1}^{ij}, \Delta U_{d3}^{ij})$ is the covariance of ΔU_{d1}^{ij} and ΔU_{d3}^{ij} ; ρ_d is the correlation coefficient of ΔU_{d1}^{ij} and ΔU_{d3}^{ij} , and can reflect the correlation strength between the axial and radial energy dissipation in a single cycle at each cycle stage.

The correlation coefficient ρ has the following properties: $|\rho| \leq 1$. if and only if there is a linear relationship between $\Delta \epsilon_{p1}^{ij}$ and $\Delta \epsilon_{p3}^{ij}$ (or ΔU_{d1}^{ij} and ΔU_{d3}^{ij}), that is $\Delta \epsilon_{p3}^{ij} = a + b\Delta \epsilon_{p1}^{ij}$ (or

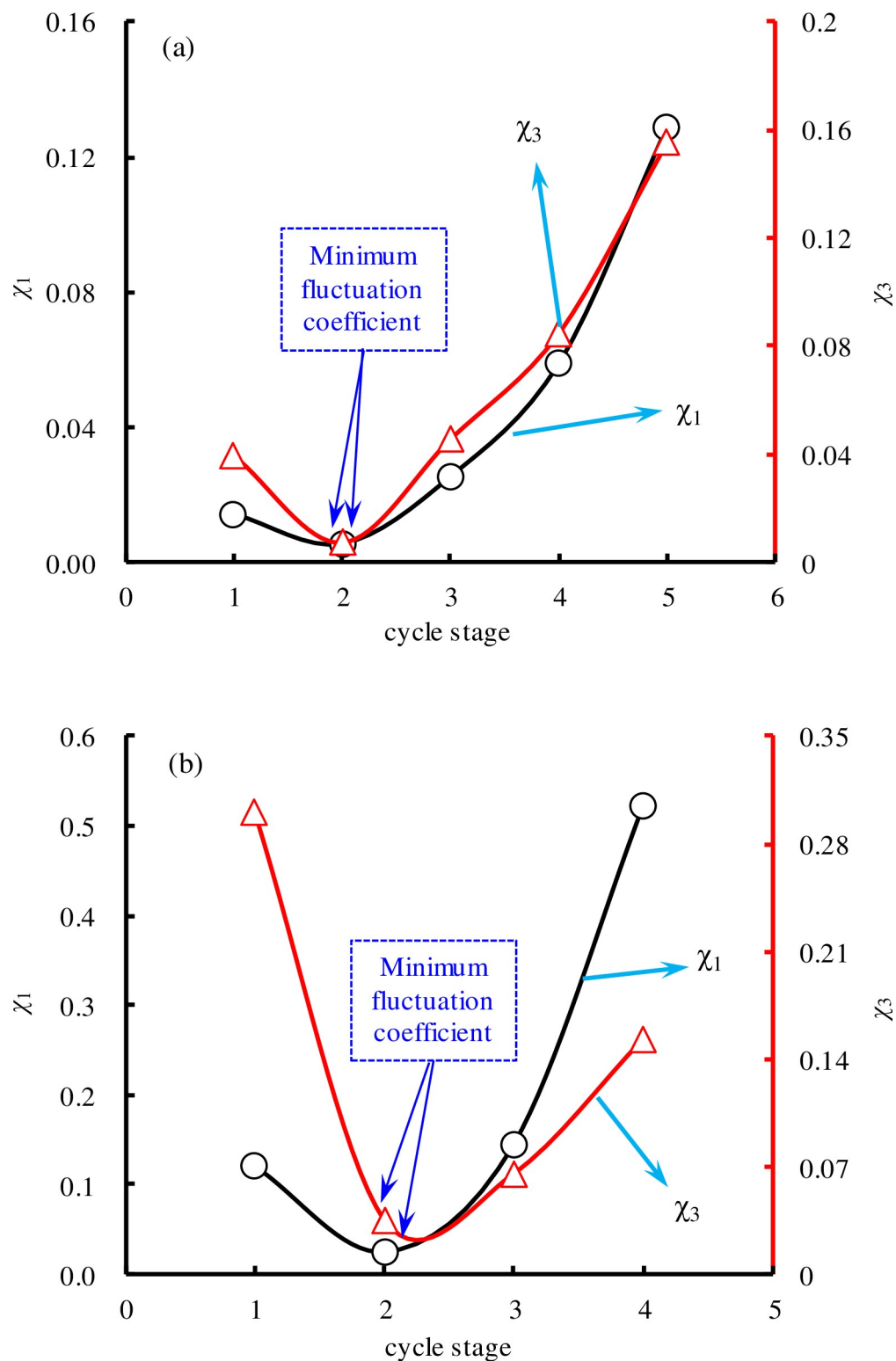


Fig 12. Fluctuation coefficient of dissipation energy in single cycle: (a) SS-1; (b) SS-2.

<https://doi.org/10.1371/journal.pone.0236335.g012>

$\Delta U_{d1}^{ij} = a + b\Delta U_{d3}^{ij}$, $|\rho| = 1$, and the following holds:

$$\rho = \begin{cases} 1, & b > 0, \\ -1, & b < 0. \end{cases} \quad (14)$$

Through the above mentioned properties, we can see that when $\rho = \pm 1$, the strongest correlation is observed between the two variables, i.e., a linear correlation. When $\rho = 0$, the two independent variables are not related. $\rho > 0$ represents a positive correlation, whereas $\rho < 0$ represents a negative correlation.

The values of ρ_p and ρ_d in each cycle stage can be calculated by Eqs (11) and (13). As shown in Fig 13, some results can be obtained, as follow. First, the changes of ρ_d and ρ_p are similar, so ρ_p can be employed as an example for detailed analysis. When $\rho_p < 0$, it indicates that $\Delta \epsilon_{p1}^{ij}$ and $\Delta \epsilon_{p3}^{ij}$ have negative correlation. With the increase of cyclic stress, ρ_p decreases first and then increases; in contrast, the correlation intensity increases first, and then decreases. In the 3th cycle stage, ρ_p reached a minimum value of -0.956 for SS-1 (or -0.931 for SS-2), i.e., the strongest correlation still did not reach -1, indicating that $\Delta \epsilon_{p1}^{ij}$ and $\Delta \epsilon_{p3}^{ij}$ were not linearly related. The mechanical behaviors of sandstone show evident nonlinear characteristics, and the integrity and coordination of the axial and radial deformations change with the stress. This is because sandstone is a natural, heterogeneous, and defective material. It contains a complex pore structure and is not an ideal elastic material. The ratio of the axial strain to the radial strain (i.e. the Poisson ratio) is not a constant but a variable under the action of force. When the stress changes, the correlation between the axial strain and radial strain also changes, and the correlation between the axial strain and the radial strain can exactly reflect the elastic plastic state or integrity of the rock. As illustrated in Fig 13, when the cyclic stress increases, the sandstone material is under constant compaction. The elasticity of the sandstone increased, the plasticity decreased, and the correlation between the axial and radial deformations was enhanced. As the cyclic stress continued to increase and exceeded the fatigue threshold stress, the sandstone fracture expanded. The plasticity of the sandstone increased, the elasticity decreased, and the correlation between the axial and radial deformation decreased. Therefore, the correlation between the axial and radial physical parameters in the rock can also be used as an index for predicting rock instability. In summary, the newly defined physical variables (ξ , χ , ρ) in this study are closely related to the elastic plastic state (or instability failure state) of rock, and can be used as indexes for predicting rock instability.

Conclusion

To study the influence of cyclic stress on nonlinear behavior in saturated sandstone, the residual strain properties and energy dissipation characteristics of sandstone under tiered cyclic loading were experimentally investigated. The axial and radial deformations and energy dissipations evolution characteristics of sandstone under cyclic loading were analyzed. In combination with the mathematical statistics, the fluctuation coefficients for the residual strain and energy dissipation, and correlation coefficients for the axial/radial residual strains and energy dissipations were defined to describe this process. The results showed that: with the increase of cycle number in each cycle stage, the values of $\Delta \epsilon_p$ and ΔU_d initially decreased rapidly, and then fluctuated near the cyclic stability line before the destruction stage. With the increase of the cycle stage, the fluctuation coefficients of $\Delta \epsilon_p$ and ΔU_d decreased first, and then increased. The correlation coefficients of the axial-radial $\Delta \epsilon_p$ and ΔU_d decreased first, and then increased. As mentioned above, the newly defined physical variables (ξ , χ , ρ) were closely related to the elastic-plastic state (or instability failure state) of the rock. Thus, they can be used as indexes for predicting rock instability.

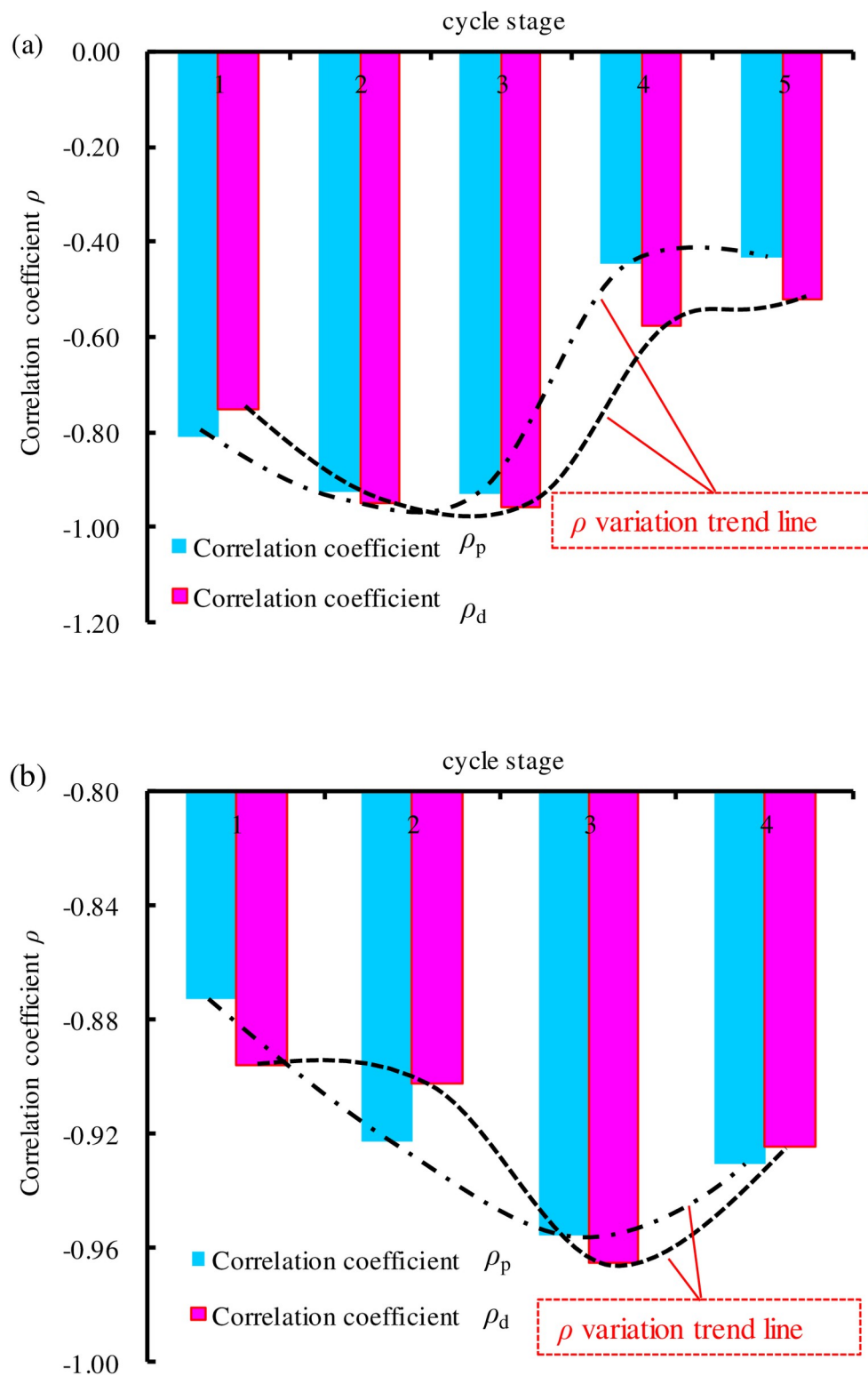


Fig 13. Correlation coefficient curve: (a) SS-1; (b) SS-2.

<https://doi.org/10.1371/journal.pone.0236335.g013>

Supporting information

S1 Data.
(ZIP)

Author Contributions

Conceptualization: Qinrong Kang.

Data curation: Minke Duan, Yang Yang.

Investigation: Guojian Cheng.

Resources: Changbao Jiang, Guojian Cheng.

Supervision: Qinrong Kang.

Writing – original draft: Minke Duan.

Writing – review & editing: Changbao Jiang, Yufei Chen.

References

1. Tutuncu AN, Podio AL, Gregory AR, Sharma MM. Nonlinear viscoelastic behavior of sedimentary rocks, Part I: effect of frequency and strain amplitude. *Leading Edge*. 1998; 63(1), 184–194
2. Zhao YX, Song HH, Liu SM, Zhang CG, Dou LM, Cao AY. Mechanical anisotropy of coal with considerations of realistic microstructures and external loading directions. *Int J Rock Mech Min Sci*. 2019; 116, 111–121.
3. Gao K, Rougier E, Guyer RA, Lei Z, Johnson PA. Simulation of crack induced nonlinear elasticity using the combined finite-discrete element method. *Ultrasonics*. 2019; 98, 51–61. <https://doi.org/10.1016/j.ultras.2019.06.003> PMID: 31200274
4. Johnson P, Sutin A. Slow dynamics and anomalous nonlinear fast dynamics in diverse solids. *J Acoust Soc Am*. 2015; 117, 124–130.
5. Shokouhi P, Riviere J, Guyer RA, Johnson PA. Slow dynamics of consolidated granular systems: Multi-scale relaxation. *Appl Phys Lett*. 2007; 111.
6. Johnson PA, Savage H, Knuth M, Gombert J, Marone C. Effects of acoustic waves on stick-slip in granular media and implications for earthquakes. *Nature* 2008; 451, 57–5. <https://doi.org/10.1038/nature06440> PMID: 18172496
7. Guyer RA, McCall KR, Boitnott GN. Hysteresis, discrete memory, and nonlinear-wave propagation in rock—A new paradigm. *Phys Rev Lett*. 1995; 74, 3491–3494. <https://doi.org/10.1103/PhysRevLett.74.3491> PMID: 10058214
8. Lu ZQ. Role of hysteresis in propagating acoustic waves in soils. *Geophys Res Lett*. 2005; 32.
9. Li TT, Pei XJ, Wang DP, Huang RQ, Tang H. Nonlinear behavior and damage model for fractured rock under cyclic loading based on energy dissipation principle. *Eng Fract Mech*. 2019; 206, 330–341.
10. Martin CD, Kaiser PK, Christiansson R. Stress, instability and design of underground excavations. *Int J Rock Mech Min Sci*. 2003; 40, 1027–47.
11. Liu XS, Ning JG, Tan YL, Gu QH. Damage constitutive model based on energy dissipation for intact rock subjected to cyclic loading. *Int J Rock Mech Min Sci*. 2016; 85, 27–32.
12. Jiang CB, Duan MK, Yin GZ, Wang JG, Lu TY, Xu J, et al. Experimental study on seepage properties, AE characteristics and energy dissipation of coal under tiered cyclic loading. *Eng Geol*. 2017; 211, 114–23.
13. Duan MK, Jiang CB, Yu H, Lu TY, Niu BW, Sun DL. Experimental research on energy dissipation and seepage properties of coal under loading-unloading conditions at different stress levels. *Rock Soil Mech*. 2018; 39(4), 1346–1354.
14. Sun B, Zhu ZD, Shi C, Luo ZH. Dynamic mechanical behavior and fatigue damage evolution of sandstone under cyclic loading. *Int J Rock Mech Min Sci*. 2017; 94, 82–89.
15. Cusumano JP, Chatterjee A. Steps towards a qualitative dynamics of damage evolution. *Int J Solids Struct*. 2000; 37, 6397–6417.

16. Hou SQ, Cai XJ, Xu JQ. A life evaluation formula for high cycle fatigue under uniaxial and multiaxial loadings with mean stresses. *Int J Mech Sci* 2015; 93, 229–239.
17. Song HP, Zhang H, Kang YL, Huang GY, Fu DH, Qu CY. Damage evolution study of sandstone by cyclic uniaxial test and digital image correlation. *Tectonophysics*. 2013; 26, 1343–1348.
18. Tong L.H, Yu Y, Xu C.J. Nonlinear dynamic behavior of cemented granular materials under impact loading. *Int J Mech Sci*. 2019; 151, 70–75
19. David E.C, Brantut N, Schubnel A, Zimmerman R.W. Sliding crack model for nonlinearity and hysteresis in the uniaxial stress–strain curve of rock. *Int J Rock Mech Min Sci*. 2012; 52(6), 9–17.
20. Bagde MN, Petroš V. Fatigue properties of intact sandstone samples subjected to dynamic uniaxial cyclical loading. *Int J Rock Mech Min Sci*. 2005; 42, 237–250.
21. Bagde MN, Petroš V. Fatigue and dynamic energy behaviour of rock subjected to cyclical loading. *Int J Rock Mech Min Sci*. 2009; 46, 200–209.
22. Araei AA, Razeghi HR, Ghalandarzadeh A. Effects of loading rate and initial stress state on stress-strain behavior of rock fill materials under monotonic and cyclical loading conditions. *Sci Iran*. 2012; 19, 1220–1235.
23. Shan PF, Lai XP, Cui F, Cao JT. Energy dissipation properties and mechanisms of fractured coal-rock mass failure under mining condition. *J Min Safety Eng*. 2018; 4, 837–839.
24. Liu HT, Qin T. Study on damage characteristics and acoustic emission Kaiser effect of sandstone under cyclic loading and unloading conditions. *Coal Sci. Technol*. 2019; 47(6), 73–80.
25. Zhong CL, Zhang ZY, Ranjith PG, Lu YY, Choi X. The role of pore water plays in coal under uniaxial cyclic loading. *Eng Geol*. 2019; 257, 105–125.
26. Peng K, Zhou JQ, Zou QL, Zhang J, Wu F. Effects of stress lower limit during cyclicloading and unloading on deformation characteristics of sandstones. *Constr Build Mater*. 2019; 217, 202–215.
27. Duan MK, Jiang CB, Xing HL, Zhang DM, Peng K, Zhang WZ. Study on damage of coal based on permeability and load-unload response ratio under tiered cyclic loading. *Arab J Geosci*. 2020; 13, 250. <https://doi.org/10.1007/s12517-020-5249-4>
28. Kumari WGP, Ranjith PG, Perera MSA, Li X, Li LH, Chen BK, et al. Hydraulic fracturing under high temperature and pressure conditions with micro CT applications: geothermal energy from hot dry rocks. *Fuel*. 2018; 230, 138–154.
29. Peng RD, Ju Y, Wang JG, Xie H, Gao F, Mao L. Energy dissipation and release during coal failure under conventional triaxial compression. *Rock Mech Rock Eng*. 2015; 48, 509–526.
30. Lu J, Yin GZ, Li X, Li MH, Zhang DM, Zhang WZ, et al. Deformation and CO₂ gas permeability response of sandstone to mean and deviatoric stress variations under true triaxial stress conditions. *Tunn Undergr Space Technol*. 2019; 84(02), 259–272.
31. Wang DK, Lv RH, Wei JP, Yao BH. An experimental study of seepage properties of gas-saturated coal under different loading conditions. *Energy Sci. Eng*. 2019; 7(3), 799–808.
32. Song ZL, Li MH, Yin GZ, Ranjith PG, Zhang DM, Liu C. Effect of Intermediate Principal Stress on the Strength, Deformation, and Permeability of Sandstone. *Energies*. 2019; 11, 2694.
33. Jiang CB, Lu TY, Zhang DM, Li GZ, Duan MK, Chen YF, et al An experimental study of deformation and fracture characteristics of shale with pore-water pressure and under triaxial cyclic loading. *R Soc Open Sci*. 2018; 5, 180670. <https://doi.org/10.1098/rsos.180670> PMID: 30225062
34. Jiang CB, Duan MK, Yin GZ, Wu GP, Yu H. Loading-unloading experiments of coal containing gas under the condition of different moisture contents. *J China Coal Society*. 2016; 41 (9), 2230–2237.
35. Xie HP, Li LY, Ju Y, Peng RD, Yang YM. Energy analysis for damage and catastrophic failure of rocks. *Sci China Tech Sci*. 2011; 54(Suppl.1), 199–209.
36. Xie HP, Li LY, Peng RD, Ju Y. Energy analysis and criteria for structural failure of rocks. *J Rock Mech Geotech Eng*. 2009; 1, 11–20
37. Duan MK, Jiang CB, Gan Q, Li MH, Peng K, Zhang WZ. Experimental investigation on the permeability, acoustic emission and energy dissipation of coal under tiered cyclic unloading. *J Nat Gas Sci Eng*. 2020; 73, 103054 <https://doi.org/10.1016/j.jngse.2019.103054>
38. Yang XL, Cao J, Cheng XY, Liu YB, Li XL, Sun ZG, et al. Mechanical response characteristics and permeability evolution of coal samples under cyclic loading. *Energy Sci Eng*. 2019; 7, 1588–1604.
39. Liu C, Yu B, Zhang D, Zhao H. Experimental study on strain behavior and permeability evolution of sandstone under constant amplitude cyclic loading-unloading. *Energy Sci Eng*. 2019; 00, 1–14.
40. Ostrovsky LA, Johnson PA. Nonlinear dynamics of rock: hysteretic behavior *Radiophys Quant El+* 2001; 44, 450–461.

41. Chen YP, Xi DY, Xue YW. Hysteresis and attenuation of saturated rocks under cyclic loading. *Chin J Geophys.* 2004; 47, 672–679.
42. Chen YP, Liu GB, Yao HL. Study of simulation for hysteretic nonlinear elasticity of rock. *Rock Soil Mech.* 2006; 27, 341–347.
43. Chen YP, Wang SJ, Wang EZ. Strength and elastic properties of sandstone under different testing conditions. *J Cent South Univ Technol.* 2007; 2, 210–215.
44. Lyakhovsky L, Hamiel Y, Ampuero P-J, Ben-Zion Y. Non-linear damage rheology and wave resonance in rocks. *Geophys J Int.* 2009; 178, 910–920.